Supporting Information

Quantifying Angular Correlations between the Atomic Lattice and Superlattice of Nanocrystals Assembled with Directional Linking

Ivan. A. Zaluzhnyy,[1,2] Ruslan P. Kurta,[3] Alexander André,[4] Oleg Y. Gorobtsov,[1] Max Rose,[1] Petr Skopintsev, [1,+] Ilya Besedin,[1,2,++] Alexey V. Zozulya,[1,3] Michael Sprung,[1] Frank Schreiber,[4] Ivan A. Vartanyants,[1,2] and Marcus Scheele[4,]*

[1]Deutsches Elektronen-Synchrotron DESY, Notkestraße 85, D-22607 Hamburg, Germany

[2]National Research Nuclear University MEPhI (Moscow Engineering Physics Institute), Kashirskoe shosse 31, 115409 Moscow, Russia

[3]European XFEL GmbH, Holzkoppel 4, D-22869 Schenefeld, Germany

[4]Eberhard Karls Universität Tübingen, Geschwister-Scholl-Platz, D-72074 Tübingen, Germany

Sample preparation

The two batches of PbS nanocrystals utilized in this study with diameters of 6.2 nm (for all X-ray experiments and the electron micrographs in **Figs. 1a-d** and 10.7 nm (for the electron micrographs in **Figs. 1e-f**) were synthesized following Weidman *et al.*[1] Neutral tetrathiafulvalene dicarboxylic acid was synthesized, deprotonated to TTFDA and used as a directional linker during a solid/air assembly of PbS nanocrystals into superlattices similar to a previously described method.[2] The sample to be coated was deposited in a tilted vial with an angle of about 20° with respect to the bench surface. The substrate was submerged in a diluted nanoparticle suspension and the vessel opening was covered to slow down evaporation. After waiting for half a day, the solution had receded, covering the substrate with multi-layered nanocrystal assemblies. The sample was covered with a solution of TTFDA (1 mg/mL in acetonitrile) for 30 min for ligand exchange. After subtraction of the ligand solution, the ligand-exchanged films were carefully washed with excess acetonitrile in order to remove excess ligand. The film thickness was estimated by scanning electron microscopy using a tilted holder. Typical thicknesses of the prepared structures were in the range between 100 – 200 nm.

For electron microscopy, copper grids coated with a thin amorphous carbon film were applied as substrates. For X-ray experiments, we utilized 5 mm x 5mm Si frames with a 500 µm x 500 µm window consisting of a 50 nm thick Si_3N_4 membrane (PLANO) as substrates.

X-ray diffraction experiment

The X-ray diffraction experiment was conducted at the Coherence Beamline P10 of the PETRA III synchrotron source at DESY. The nanodiffraction endstation GINIX was used to focus an X-ray beam with energy $E = 13.8$ keV (λ = 0.898 Å) down to 400 x 400 nm^2 size with KB-mirrors.[3] The depth of the X-ray focus was about 0.5 mm. The sample was

positioned perpendicular to the incoming X-ray beam, and an area of 13.6 x 20 μm^2 was scanned to analyze the spatial variations of the samples' structure. Within this scanning region, 1785 diffraction patterns were collected on the 34 x 50 raster grid with a 400 nm step size in both directions. Each diffraction pattern was collected with an exposure time of 0.5 s to prevent radiation damage, which was confirmed by repeating the scanning procedure several times on the same position of the sample. A two-dimensional detector Pilatus 1M (981x1043 pixels of 172x172 μm^2 size) was positioned downstream at a distance of 46 cm from the sample and shifted approximately by 8 cm to the side (**Fig. 2**). In such geometry, we were able to detect the scattering signal from the SL as well as from PbS AL simultaneously. Only a part of reciprocal space in wide angle scattering was accessible with the detector. The detector resolution of SAXS was about 0.03 nm^{-1} and in the region of WAXS – approximately 0.02 nm^{-1}. The measured signal was corrected for background scattering.

X-ray cross-correlation analysis

The CCFs $C(q_1, q_2, \Delta)$ were calculated according to the equation

$$C(q_1, q_2, \Delta) = \frac{1}{2\pi} \int_{-\pi}^{\pi} I(q_1, \varphi) I(q_2, \varphi + \Delta) d\varphi,$$

where $I(q, \varphi)$ is expressed in polar coordinates on the detector plane, q_1 and q_2 are two magnitudes of the momentum transfer vectors, φ is an angular coordinate around a diffraction ring, $-\pi < \Delta \leq \pi$ is an angular variable (**Fig. 2**). To obtain statistically meaningful data, CCFs were averaged over a large number of measured diffraction patterns

$$\langle C(q_1, q_2, \Delta) \rangle_M = \frac{1}{M} \sum_{i=1}^{M} C^i(q_1, q_2, \Delta) .$$

Here index i enumerates diffraction patterns, M is total number of measured diffraction patterns and $\langle ... \rangle_M$ denotes ensemble averaging.[4]

In the present work, the scattered signal in the WAXS region was limited by the detector size. In this case, one can still evaluate two-point CCF $C(q_1, q_2, \Delta)$ by applying a mask $W(q, \varphi)$, which is equal to unity in the regions where the scattering signal was measured and to zero outside of the detector. Using such a mask allows one to consider only a pair of points in the CCF that both lie within the detector area. In this case, the CCF should be evaluated as

$$C(q_1, q_2, \Delta) = \frac{\int_{-\pi}^{\pi} I(q_1, \varphi) W(q_1, \varphi) I(q_2, \varphi + \Delta) W(q_2, \varphi + \Delta) d\varphi}{\int_{-\pi}^{\pi} W(q_1, \varphi) W(q_2, \varphi + \Delta) d\varphi}.$$

In our work, the signal in the SAXS region was recorded by the detector completely, so $W(q_4^{SL}, \varphi) = 1$, except for the region shadowed by the beamstop holder, where $W(q_4^{SL}, \varphi) = 0$. In the WAXS region the mask $W(q_{111}^{AL}, \varphi)$ was set to zero outside the detector (for $\varphi \lesssim -45°$ and $\varphi \gtrsim 45°$) and in the region of detector gaps. For all other points, $W(q_{111}^{AL}, \varphi) = 1$.

Analysis of the angular averaged signal in SAXS region

In order to determine the structure of the SL we performed analysis of the angular averaged scattered signal in the SAXS region. After subtraction of a measured background from the diffraction data and integration over the azimuthal variable φ, we obtained a q-dependence of the SAXS signal $I(q)$, which is shown in **Fig. S1a**. We observe four scattering peaks from the SL at $q_1^{SL} = 0.98\ \mathrm{nm}^{-1}$, $q_2^{SL} = 1.08\ \mathrm{nm}^{-1}$, $q_3^{SL} = 1.34\ \mathrm{nm}^{-1}$ and $q_4^{SL} = 1.72\ \mathrm{nm}^{-1}$. The first two peaks are not resolved completely, if the signal averaged over all measured diffraction patterns is considered. However, on individual diffraction profiles two peaks at q_1^{SL} and q_2^{SL} are well distinguished. We attribute these peaks to the {011}, {110}, {002} and {112} families of reflections of bcc lattice with tetragonal distortion. If we fix the value of the

tetragonal distortion obtained from XCCA ($c/a \approx 1.22$), the best fitting of the diffraction peak positions was obtained for a bct structure with unit cell parameters $a = b = 7.9 \pm 0.4$ nm and $c = 9.7 \pm 0.4$ nm (for such a lattice $q_1^{SL} = 1.03\ \mathrm{nm}^{-1}$, $q_2^{SL} = 1.13\ \mathrm{nm}^{-1}$, $q_3^{SL} = 1.30\ \mathrm{nm}^{-1}$ and $q_4^{SL} = 1.72\ \mathrm{nm}^{-1}$)

Due to the inhomogeneity of the sample and imperfections of the SL, the determination of SL unit cell parameters becomes challenging. In **Fig. S1b** the q-positions of the {011}, {110}, {002} and {112} reflections are shown as a function of the diffraction pattern number. It is clearly visible that these values fluctuate depending on the position on the sample, which means that the structure of the SL is slightly position-dependent. In **Figs. S1(c-d)** two spatially resolved maps represent how the unit cell parameters a and c of the bct superlattice change depending on position on the sample. Within the domains marked in **Figs. S1(c-d)** with white lines the values of the bct lattice parameters are $a = b = 8.1 \pm 0.4$ nm and $c = 9.5 \pm 0.3$ nm, that is in good agreement with values obtained from XCCA analysis.

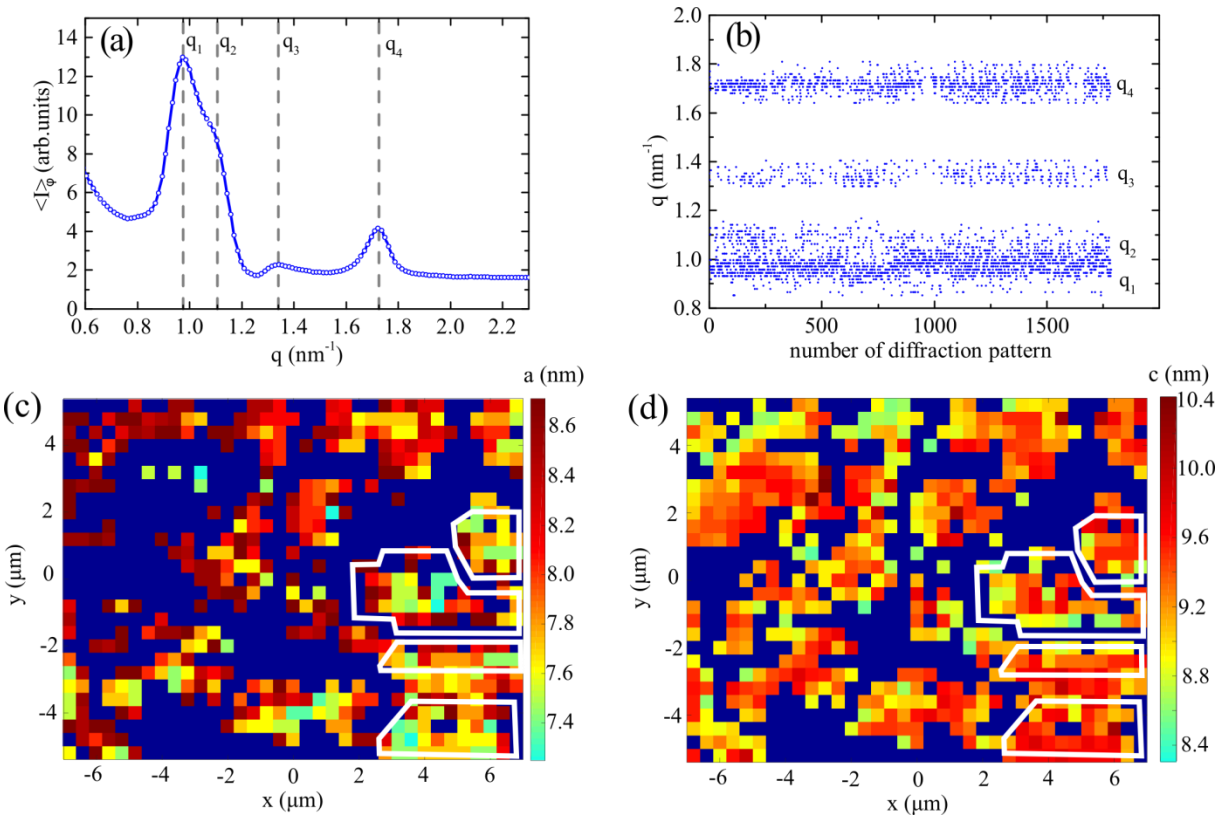

Figure S1. a) *The q-dependence of the angular averaged intensity* $\langle I(q,\varphi)\rangle_{\varphi}$. ***b)*** *q-position of the scattering peaks for different individual diffraction patterns.* ***c)-d)*** Spatially resolved map of bct superlattice parameters a (**c**) and c (**d**). The domains (see **Fig. 4**) are shown with white lines.

Evaluation of angle 2β between two $\{112\}_{SL}$ peaks for the bct structure

The unit cell of the bct structure is based on three orthogonal vectors $\boldsymbol{a}$, $\boldsymbol{b}$ and $\boldsymbol{c}$ with moduli $|\boldsymbol{a}| = |\boldsymbol{b}| = a$ and $|\boldsymbol{c}| = c$ (see **Fig. S2a**). Corresponding vectors of the reciprocal lattice are also orthogonal, so the Gram matrix for the reciprocal space is

$$G = \begin{pmatrix} 2\pi/a^2 & 0 & 0 \\ 0 & 2\pi/a^2 & 0 \\ 0 & 0 & 2\pi/c^2 \end{pmatrix}. \quad (1)$$

A diffraction pattern from a bct lattice oriented in such a way that the [110] direction is parallel to the incident X-ray beam is shown in **Fig. S2b**. The angle 2β between two Bragg peaks from {112} reflections can be evaluated as

$$\cos 2\beta = \frac{u^T G v}{\sqrt{u^T G u}\sqrt{v^T G v}}, \quad (2)$$

where $u^T = (1\ -1\ 2)$ and $v^T = (-1\ 1\ 2)$ are the indexes of two reflections and T denotes transposition. Substituting the Gram matrix (1) into Eq. (2) and solving the obtained equation for the angle β yields

$$\tan\beta = \frac{c}{a\sqrt{2}}. \quad (3)$$

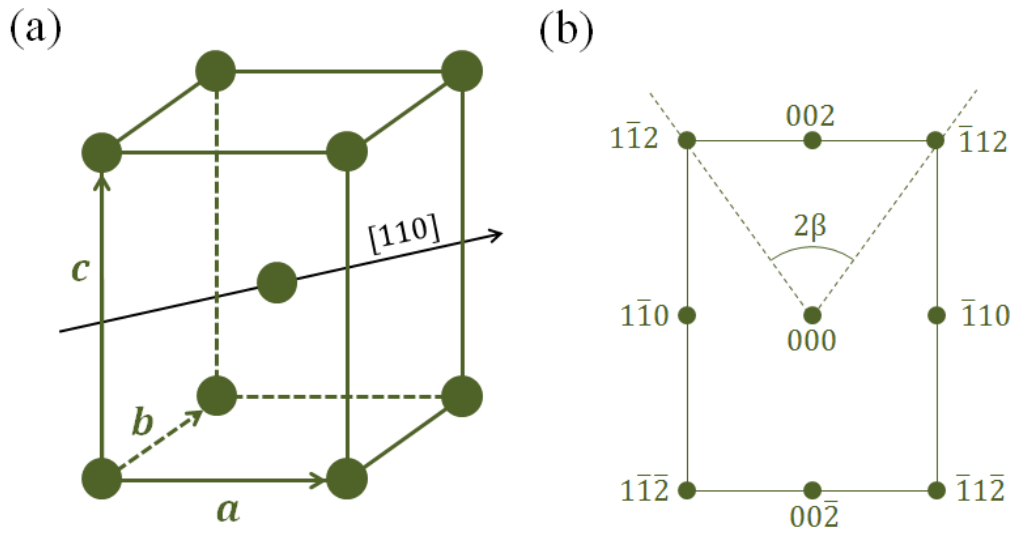

Figure S2. a) *Unit cell of the bct structure.* ***b)*** *Positions of the Bragg peaks from the bct structure if [110] direction is parallel to the beam.*

Spatially resolved map of misorientation between the superlattice and atomic lattice

At many positions on the sample, one can unambiguously determine both orientations of SL and AL (see spatially resolved maps in **Figs. 4a-b**). For these positions, we can directly calculate a mismatch between the angular orientation of SL and AL. Let us assume that the directions $[110]_{AL}$ and $[110]_{SL}$ coincide and they are perpendicular to the sample surface. In this case, both SL and AL can rotate around this axis. Thus, we can measure an angular mismatch ψ between SL and AL by considering an angle between $[001]_{AL}$ and $[001]_{SL}$ directions (or equivalent angle between $[1\bar{1}0]_{AL}$ and $[1\bar{1}0]_{SL}$ directions). In case of perfect alignment this angle is equal to zero, and it can be positive or negative depending on the direction in which PbS particles are rotated with respect to SL (see **Fig. S3a**).

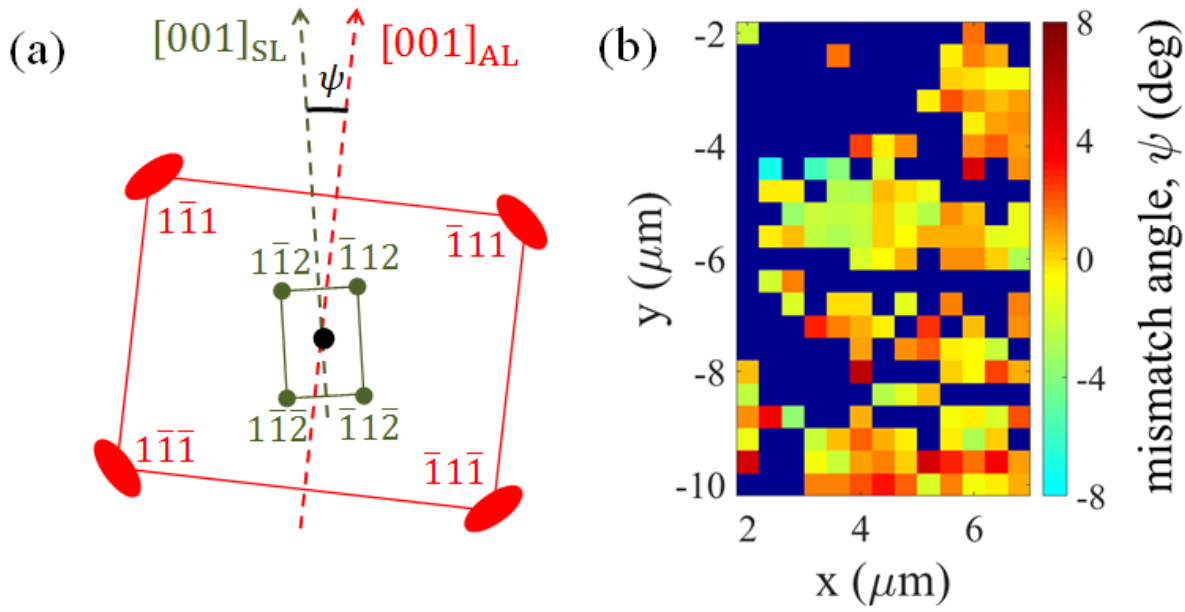

Figure S3. a) *Schematic representation of reciprocal space. Diffraction peaks from the AL are shown with red color, and diffraction peaks from the SL are shown with green color. A mismatch angle ψ between* $[001]_{AL}$ and $[001]_{SL}$ directions *represents misalignment between SL and AL.* ***b)*** *Spatially resolved map showing the angular mismatch between orientations of SL and AL. Dark blue regions correspond to points on the sample where orientation of the SL or AL, or both, could not be determined. Typically, the angular mismatch between SL and AL lies in the range from -2.5° to 2.5°.*

The spatially resolved map of the mismatch angle ψ for some region of the sample is shown in **Fig. S3b**. Different values of the angle are represented by different colors, and dark blue color corresponds to the regions, where the mismatch angle could not be obtained, due to absence of scattering signal or ambiguity in determination of SL or AL orientation. The mean value of the mismatch angle is equal to approximately 0.1°, which indicates that PbS nanoparticles can be rotated in any direction with respect to the SL (otherwise the mean value would significantly differ from zero). The standard deviation for the mismatch angle is about 2.5°, indicating that the PbS nanoparticles are aligned with respect to the SL and can only slightly be rotated around the preferred orientation within an angle of few degrees.

On the effect of orientational disorder between atomic lattices

If all atomic lattices were perfectly aligned with respect to each other, the PbS [110] direction would be precisely parallel to the incident X-ray beam for all atomic lattices. In such a case, the Ewald sphere does not intersect with the PbS {111} Bragg reflections, even upon taking into account the finite size of the PbS nanocrystals and the associated broadening of the Bragg peaks. In general, angular disorder of the AL relative to the SL should be characterized by two angles, $\Delta\Phi_{az}$ and $\Delta\Phi_{pol}$, which will cause broadening of the PbS {111} reflections (see **Fig. S4**). In our experiment $\Delta\Phi_{pol} \neq 0$, so significant intersection with the Ewald sphere is possible for most nanocrystals albeit the general [110] orientation. This is why the {111} Bragg peaks are indeed frequently observed by us (see **Fig. 3a-d**). Elongated shape of the diffraction peaks in azimuthal direction (see **Fig. 3e**) implies $\Delta\Phi_{az} \neq 0$. Since it is impossible to distinguish effects of these two angles by analysis of diffraction patterns only in transmission geometry, we assumed that $\Delta\Phi_{az} \approx \Delta\Phi_{pol} \approx \Delta\Phi$, that allows us to characterize the angular disorder by a single value $\Delta\Phi$.

To quantitatively characterize angular disorder we assumed that the width of the 111 AL diffraction peaks in radial direction is determined only by Sherrer broadening, and the width in azimuthal direction is determined by Sherrer broadening as well as angular disorder (see **Fig. 3** (e-g)). Thus, the azimuthal profile of the Bragg peaks can be described as a convolution of its radial profile and orientational distribution function. Therefore one can write $(\Delta q_{az})^2 = (\Delta q_{rad})^2 + (\Delta q_{\Delta\Phi})^2$, where Δq_{az} and Δq_{rad} are FWHM of the diffraction peak in azimuthal and radial directions, respectively, and $\Delta q_{\Delta\Phi}$ is broadening of the diffraction peak in radial direction caused by orientational disorder. In this case, the value of $\Delta\Phi$ can be estimated as $\Delta\Phi = \Delta q_{\Delta\Phi}/q_{111}^{AL} \approx 10°$.

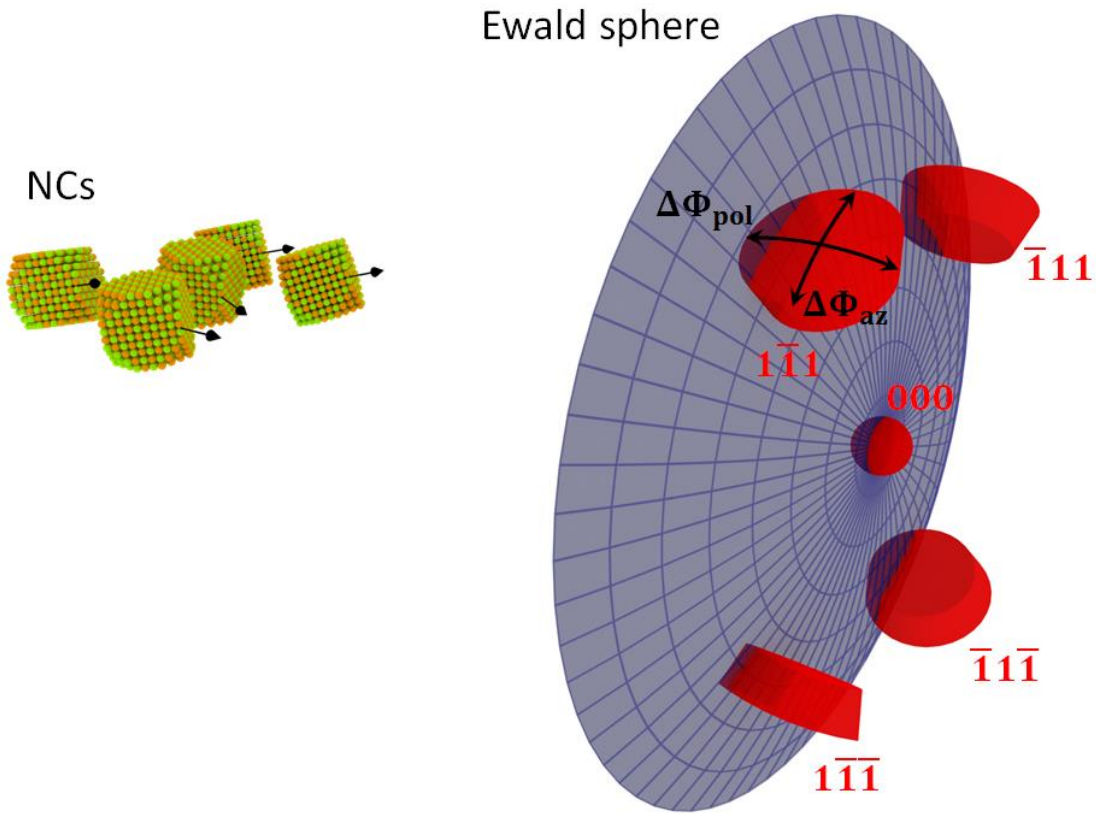

Figure S4. Scheme of reciprocal space with the $\{111\}_{AL}$ reflection from PbS in case of orientational disorder in the atomic lattice. The Ewald sphere is shown in blue color, and Bragg peaks are depicted in red color. Bragg reflections $\{111\}_{AL}$ are broadened in two orthogonal directions due to orientational disorder $\Delta\Phi_{az}$ and $\Delta\Phi_{pol}$.

Evaluation of the model cross-correlation function

For a realistic model of the experimental conditions, it is not enough to take into account the size of the detector that limits the measured scattering signal in the WAXS region. One also has to consider the fact that the sample can be oriented differently with respect to the detector. Thus, an angle δ between the $[1\bar{1}0]_{AL}$ direction of the AL and direction $\varphi = 0$ is not necessarily equal to zero (see **Fig. 5b**). Moreover, this angle can vary from one diffraction pattern to another. Due to that we calculated the model CCF as an average over all possible values of angle δ

$$C_{model}(\Delta) = \frac{1}{\sqrt{2\pi\sigma_\delta^2}} \int_{-\pi}^{\pi} C(\Delta,\delta) exp\left[-\frac{1}{2}\frac{(\delta-\delta_0)^2}{\sigma_\delta^2}\right] d\delta. \qquad (4)$$

Here, we assume a normal distribution of the angle δ. The best fit with the experimental CCF was obtained for the standard deviation $\sigma_\delta = 0.15$ (8.6°) and mean $\delta_0 = 0.045$ (2.6°). A non-zero value of parameter δ_0 indicates that the sample was misaligned with respect to the detector. The CCF $C(\Delta,\delta)$ was obtained according to the following procedure

$$C(\Delta,\delta) = \frac{\int_{-\pi}^{\pi} I_{WAXS}(\varphi,\delta) W_{WAXS}(\varphi) I_{SAXS}(\varphi+\Delta,\delta) W_{SAXS}(\varphi+\Delta) d\varphi}{\int_{-\pi}^{\pi} W_{WAXS}(\varphi) W_{SAXS}(\varphi+\Delta) d\varphi}. \qquad (5)$$

Here $W_{WAXS}(\varphi)$ and $W_{SAXS}(\varphi)$ are masks in the WAXS and SAXS regions, respectively. The intensity of the WAXS peaks is modeled by a sum of Lorentzian functions

$$I_{WAXS}(\varphi,\delta) = A_{WAXS} \sum_{i=1}^{4} \frac{\gamma_{WAXS}^2}{\left(\varphi-\delta-\varphi_{WAXS}^i\right)^2 + \gamma_{WAXS}^2}, \qquad (6)$$

where $A_{WAXS} = 2.3$ is a constant scaling factor, $\gamma_{WAXS} = 0.09$ (5.2°) is the half width at half maximum of a diffraction peak. If the coordinate system is introduced as shown in **Fig. 5b,** the angular positions of the 111_{AL} diffraction peaks in WAXS region are $\varphi_{WAXS}^i = \{-\pi+\theta, -\theta,\ \theta,\ \pi-\theta,\} \approx \{-144.74°, -35.26°, 35.26°, 144.74°\}$, where $\theta = \arctan\left(\frac{1}{\sqrt{2}}\right)$. The intensity from the bct structure along the [110] zone axis, $I_{SAXS}(\varphi)$, was modelled in the same way as a sum of four Lorentzian peaks

$$I_{SAXS}(\varphi,\delta) = A_{SAXS} \sum_{i=1}^{4} \frac{\gamma_{SAXS}^2}{\left(\varphi-\delta-\varphi_{SAXS}^i\right)^2 + \gamma_{SAXS}^2}, \qquad (7)$$

where $A_{SAXS} = 17$, $\gamma_{SAXS} = 0.03$ (1.7°), $\varphi_{SAXS}^i = \{-\pi/2-\beta, -\pi/2+\beta, \pi/2-\beta, \pi/2+\beta\}$, and β is an adjustable parameter. To simulate experimental conditions, we also added a noise to $I_{WAXS}(\varphi,\delta)$ and $I_{SAXS}(\varphi,\delta)$, modelled as a uniformly distributed signal in the range

from -2 to 2. Using the values indicated above for the angular positions of the diffraction peaks in Eqs. (6) and (7), we assumed that the SL and AL are perfectly aligned with respect to each other, i.e. $\psi = 0$. Fitting the positions of the model CCF peaks to the experimentally obtained values yields $\beta = 40.7°$.

In the experiment, we were able to measure simultaneously the signal in the SAXS region for all azimuthal angles, however in the WAXS region we were restricted by the detector size and measured the scattering signal only in the angular range of approximately 90° azimuthally. To simulate the effect of finite detector size we used the following mask for the WAXS signal

$$W_{WAXS}(\varphi) = \begin{cases} 1, & -45° < \varphi < 45° \\ 0, & \text{otherwise} \end{cases}, \quad (8)$$

while $W_{SAXS}(\varphi) \equiv 1$ for $-180° \leq \varphi < 180°$. To represent the effect of the detector gaps, beamstop and shadow from the beamstop holder, we also set these points to zero in $W_{WAXS}(\varphi)$ and $W_{SAXS}(\varphi)$.

References:

(1) Weidman, M. C.; Beck, M. E.; Hoffman, R. S.; Prins, F.; Tisdale, W. A. *ACS Nano* **2014**, *8* (6), 6363–6371.

(2) André, A.; Zherebetskyy, D.; Hanifi, D.; He, B.; Samadi Khoshkhoo, M.; Jankowski, M.; Chasse, T.; Wang, L.-W.; Schreiber, F.; Salleo, A.; Liu, Y.; Scheele, M. *Chem. Mater.* **2015**, *27* (23), 8105–8115.

(3) Salditt, T.; Kalbfleisch, S.; Osterhoff, M.; Krüger, S. P.; Bartels, M.; Giewekemeyer, K.; Neubauer, H.; Sprung, M. *Opt. Express* **2011**, *19* (10), 9656–9675.

(4) Kurta, R. P.; Altarelli, M.; Vartanyants, I. A. In *Advances in Chemical Physics*; John Wiley & Sons, Inc., 2016; pp 1–39.